Acta Cryst. (1995). A51, 504–514

Contrast of HOLZ Lines in Energy-Filtered Convergent-Beam Electron Diffraction Patterns from Silicon

BY G. LEHMPFUHL, D. KRAHL AND Y. UCHIDA

Fritz-Haber-Institut der Max-Planck-Gesellschaft, Faradayweg 4-6, *D*-14195 *Berlin, Germany*

(*Received* 16 *September* 1994; *accepted* 12 *December* 1994)

Abstract

Higher-order Laue-zone (HOLZ) lines were investigated in convergent-beam electron diffraction patterns from silicon near the low-indexed zone axes [100], [110] and [111]. The visibility of these lines depends on the effective structure potentials of the reflections from the first Laue zone depending on their Debye–Waller factor. The contrast of the HOLZ lines is strongly reduced by inelastically scattered electrons. They can be excluded by an imaging Ω filter for energy losses above 2 eV. The diffraction patterns were compared with many-beam calculations. Without absorption, an excellent agreement could be achieved for the [111] and [100] zone axes, while the simulation of the [110] zone-axis pattern needed a calculation with absorption. The reason for this observation is explained in the Bloch-wave picture. Calculations with absorption, however, lead to artefacts in the intensity distribution of the [100] HOLZ pattern. In order to obtain agreement with the experiment, the Debye–Waller factor had to be modified in different ways for the different zone axes. This corresponds to a strong anisotropy of the Debye–Waller factor. To confirm this observation, the temperature dependence of the itensity distributions of the HOLZ patterns was investigated between 50 and 680 K. At room temperature, the parameter D in the Debye–Waller factor $\exp(-Ds^2)$ was determined as 0.13, 0.26 and 0.55 Å^2 for the zone axes [100], [111] and [110], respectively. The reliability of the conclusions is discussed.

Introduction

Large-angle convergent-beam electron diffraction patterns, called Kossel patterns for electrons (Goodman, 1974), are similar to Kikuchi patterns which are formed by inelastically scattered electrons. They contain more information on the crystal structure than Kikuchi patterns. Since the Kikuchi patterns consist of electrons of different energies, information is lost. The convergent-beam patterns contain, as well as the elastically scattered electrons, inelastically scattered electrons which may cover important features of elastic scattering. When an energy filter (Krahl, 1990) is used for imaging the diffraction pattern, the inelastically scattered electrons can be cut off above an energy-loss level given by the resolution of the filter (Holmestad, Krivanek, Høier, Marthinsen & Spence, 1993). This allows an accurate analysis of the diffraction pattern by simulation (Mayer, Spence & Möbus, 1991).

Convergent-beam electron diffraction patterns show, near low-indexed zone axes, faint lines resulting from reflections of the first Laue zone. These lines are called 'higher-order Laue-zone' (HOLZ) lines (Steeds & Jones, 1975; Rackham, Steeds & Jones, 1975). They contain three-dimensional information on lattice parameters and energy of the incident electrons, as demonstrated by Tanaka, Terauchi & Kaneyama (1985). Their intensity depends on the effective structure potential of the corresponding reflections. By 'effective', the influence of the Debye–Waller factor is meant. This results in a temperature dependence of the intensity of the HOLZ lines.

In this work, we will test what information can be obtained by comparing energy-filtered HOLZ patterns with calculated intensity distributions using the formalism of the dynamical theory of electron diffraction described, for example, in the papers of Voss, Lehmpfuhl & Smith (1980) and Kambe & Molière (1970).

Experiment

Experiments were performed with silicon near the three zone axes [111], [100] and [110]. Specimen discs in these orientations were prepared by cutting, dimple grinding and subsequent ion thinning or chemical etching.

In order to exclude the inelastically scattered electrons at room temperature, a Siemens Elmiscope with an Ω filter was used (Krahl, 1990). The diffraction patten was built up mainly by elastically scattered electrons and electrons that had suffered energy losses of less than 2 eV. The condition for convergent-beam electron diffraction (Goodman & Lehmpfuhl, 1965) from a small specimen area of several tens of nanometres diameter was achieved by lowering the z position of the specimen. The cone angle of the incident beam could be adjusted by a combination of the lens currents for the condenser, objective and intermediate lens in such a way that neighbouring diffraction discs were just touching each

ISSN 0108-7673

other. These lens currents depend on the size of the condenser aperture. The crystals were mounted on a top-entry double-tilt goniometer stage. In order to reduce the contamination, the area around the specimen was cooled by liquid nitrogen.

The temperature dependence of the intensity distribution in the zone-axis patterns was investigated with different electron microscopes. The DEEKO 250 with a cryo-goniometer stage, developed in our institute (Heide, 1982), was used to cover the temperature range between room temperature and 10 K. For elevated temperatures, the Philips 400T was used with a Gatan heating double-tilt goniometer stage. With the Siemens Elmiscope, energy filtering could only be done at room temperature. Comparison with unfiltered patterns indicates the gain in information one could expect by filtering at lower or more elevated temperatures.

Experimental results

In the [111] zone-axis pattern, the strongest influence of the first Laue zone can be seen in an energy-filtered pattern, as shown in Fig. 1(*a*). In this well known pattern, a very strong contrast of the HOLZ lines is observed because the inelastically scattered electrons with energy losses above approximately 2 eV are excluded. The fine lines with threefold symmetry are due to the reflections from the first Laue zone. The wide extinction contours with sixfold symmetry are due to the reflections from the zeroth Laue zone and depend on the crystal thickness. Fine details in the centre and subsidiary maxima between HOLZ lines can clearly be seen. Without filtering, the contrast is strongly reduced, as shown in Fig. 1(*b*). The reduction of contrast by contamination could be excluded in this case. The change of contrast with temperature is shown in Fig. 1(*c*) at 100 K and in Fig. 1(*d*) at 660 K without filtering. At these temperatures, the contamination is strongly reduced. Only inelastically scattered electrons contribute to the background.

HOLZ lines in the [100] zone-axis pattern are more faint because the scattering angles of reflections of the first Laue zone are larger than those in the [111] zone axis, and consequently the structure potentials of the corresponding reflections are weaker. However, by energy filtering they become visible with good contrast, as shown in Fig. 2(*a*). Without filtering, their contrast is poor, as can be seen in Fig. 2(*b*). The change of contrast with temperature is shown in Fig. 2(*c*) at 20 K and in Fig. 2(*d*) at 430 K. At the low temperature, the contrast of the HOLZ lines becomes very strong, even without filtering. At the high temperature, the HOLZ lines have almost disappeared.

In the [110] zone-axis pattern, the HOLZ lines are not visible at room temperature, even after energy filtering, as shown in Fig. 3(*a*). The intensity of the reflections of the first Laue zone is too weak to modify the intensity distribution owing to the reflections from the zeroth Laue zone. The indices of the HOLZ refelctions are very large, as discussed in the *Concluding remarks*. The characteristic intensity distribution is therefore determined only by reflections of the zeroth Laue zone. When the temperature is lowered, faint HOLZ lines become visible at 50 K, as shown in Fig. 3(*b*). The contrast is reduced by inelastically scattered electrons since energy filtering could only be done at room temperature.

Calculation

The convergent-beam diffraction patterns were compared with simulations, as described by Voss, Lehmpfuhl & Smith (1980) using the Bethe formulation of dynamical theory with structure potentials from Doyle & Turner (1968). For the low-indexed structure potentials, the experimentally refined values from Voss, Lehmpfuhl & Smith (1980) have been used. The zero-beam intensity was calculated in a many-beam approximation with up to 180 beams for a field of 128 × 128 points of different directions of incidence. Similar simulations near the [111] zone axis for the zero beam and several reflections have been already performed by Zhou (1991) and Zhou & Möllenstedt (1992).

The absorption, introduced as an imaginary part of the structure potential by Molière (1939), was described by a model by Humphreys & Hirsch (1968), confirmed by Voss, Lehmpfuhl & Smith (1980), and can be expressed in a quadratic approximation as

$$Vg_{\text{im}} = Vg_{\text{real}}(Ag - Bg^2) \qquad (1)$$

for small scattering angles. g^2 is the sum of the squares of the reflection indices. However, for larger scattering angles, as in the case of reflections from the first Laue zone, for which the expression in parentheses would become negative, an exponential expression due to Ichimiya & Lehmpfuhl (1978) is more correct:

$$Vg_{\text{im}} = C\exp(-Fg^2)\{\text{lattice factor}\}. \qquad (2)$$

For silicon, the constants in (1) and (2) are: $A = 0.004$, $B = 0.0003$, $C = 0.0062$ V and $F = 3.8$.

The Debye–Waller factor used in the calculation for the reduction of the structure potentials is given in the form (*e.g.* Reimer, 1989)

$$\exp(-Ds^2) \qquad (3)$$

with $s = (h^2 + k^2 + l^2)^{1/2}/2a$, where $a = 5.43$ Å is the lattice constant of silicon and D is the parameter in Å^2 that is determined by comparison of experiment with simulation. In several simulations, the absorption potential (2) was multiplied by the Debye–Waller factor (3).

As mentioned above, the calculations were performed for a field of 128 × 128 points of different directions of incidence. For each direction of incidence, the relevant reflections were selected according to the value of their

excitation error divided by their structure potential. One problem arises from the fact that reflections of the first Laue zone do not have their intensity maximum at zero excitation error owing to dynamical interactions, which can be understood as a kind of refraction. In the case of an insufficient number of beams, relevant HOLZ reflections can be missed in a calculation by the selection procedure. In calculations where forbidden reflections from the zeroth Laue zone have to be included, the excitation errors for reflections from the zeroth Laue zone were divided by a constant value corresponding to a low-indexed structure potential, *e.g.* 2.0 V, while only the

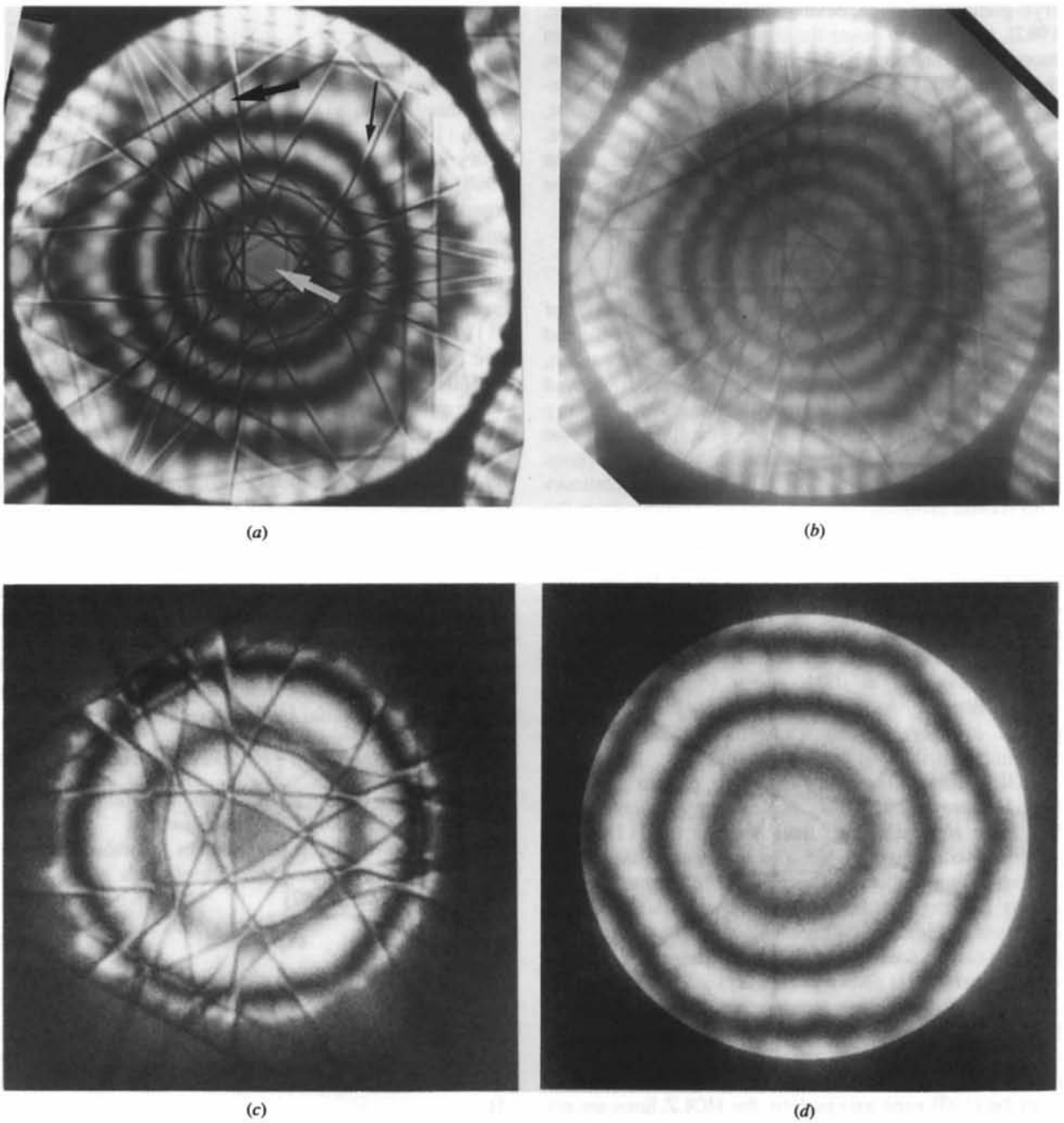

Fig. 1. (*a*) Zero beam of a convergent-beam pattern near the [111] zone axis with HOLZ lines of the first Laue zone. Elastic pattern after filtering at room temperature. Electrons with energy losses above 2 eV are excluded. The energy of the electrons is 100 keV. The arrows indicate details described in the text. (*b*) Si [111] HOLZ pattern without filtering; the inelastic contribution reduces the contrast of the HOLZ lines. (*c*) Si [111] HOLZ pattern without filtering at 100 K. (*d*) Si [111] HOLZ pattern without filtering at 660 K.

excitation errors of reflections from the first Laue zone were divided by their structure potential. This selection procedure appears to cause some remaining problems.

Comparison of experiment with simulation

Comparison of the geometrical arrangement of calculated HOLZ lines with experimental observations allows an accurate determination of the energy of the electrons (within a fraction of a percent) and comparison of their intensity distribution allows the determination of the Debye–Waller factor. From intensity distributions due to the zero-order Laue zone, the crystal thickness can be determined. An approximate value is obtained from the distribution of the wide extinction contours. It should be mentioned here that the Debye–Waller factor, low-

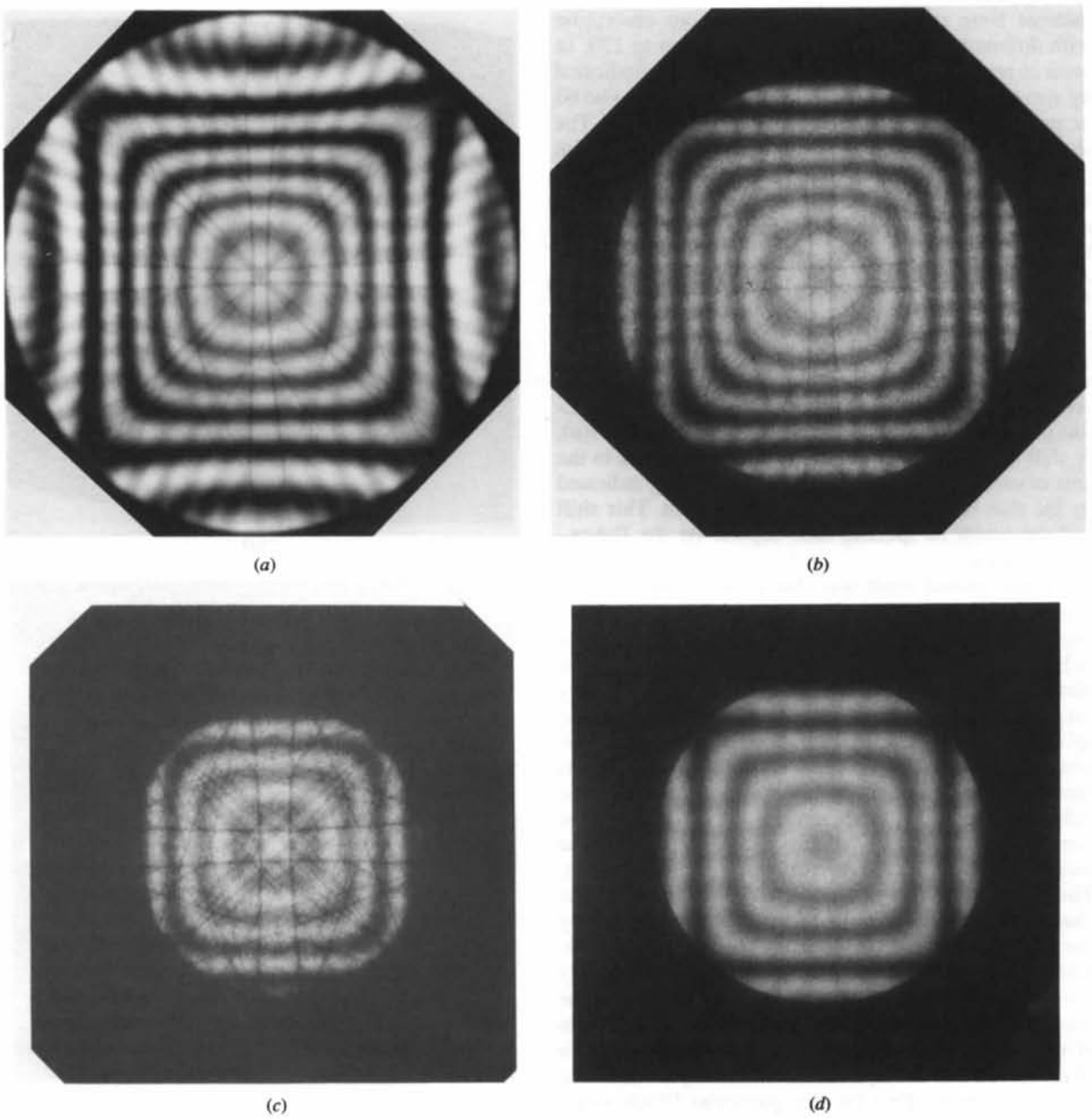

Fig. 2. (*a*) Zero beam of a convergent-beam pattern near the [100] zone axis with HOLZ lines from the first Laue zone after energy filtering at room temperature. Electrons with energy losses above 2 eV are excluded. (*b*) Si [100] HOLZ pattern without energy filtering at room temperature. (*c*) Si [100] HOLZ pattern without filtering at 20 K. (*d*) Si [100] HOLZ pattern without filtering at 430 K.

indexed structure potentials and model of absorption have an influence on the position of the wide extinction contours.

The results of the simulation of HOLZ patterns for the three main zone axes [111], [100] and [110] are shown below.

[111] *patterns*

The strongest influence of the first Laue zone is found in the [111] HOLZ pattern in Fig. (1*a*). The [111] HOLZ patterns were calculated with and without absorption with different numbers of beams from 30 up to 120. In order to reproduce certain details in the pattern, indicated by arrows in Fig. 1(*a*), the number of beams had to be 60 or more. Above 90 beams, the results converge. The absorption potential due to Voss, Lehmpfuhl & Smith (1980) was used in the form of (2). Best agreement with the experiment could be obtained at room temperature in a 90-beam calculation with $D = 0.26\,\text{Å}^2$ in (3), shown in Fig. 4(*a*), instead of $D = 0.46\,\text{Å}^2$, which was used by Aldred & Hart (1973). The thickness is slightly different from the experiment in Fig. 1(*a*) but the thickness contours due to the zeroth Laue zone have no influence on the geometry of the HOLZ lines. The reproduction shows very fine details as subsidiary maxima in the centre, indicated by the white arrow, or between HOLZ-line pairs, indicated by the thick black arrow in Fig. 1(*a*). A shift of the zero Laue-zone extinction contours in the area of crossing HOLZ lines and their splitting, indicated by the thin black arrow, can clearly be seen. This shift and the width of splitting also depend on the Debye–Waller factor.

An unexpected result was that with no absorption or only a mean absorption good agreement between experiment and calculation could be obtained, as shown in Fig. 4(*b*). The calculation reproduces fine details in the intensity distribution very well, such as the subsidiary maxima in the centre or between HOLZ lines. Only the splitting of the HOLZ lines when crossing the extinction contours, indicated by the thin black arrow in Fig. 1(*a*), is reproduced better in a calculation with absorption and the reduced value of D. Here, the question arises why the simulation of HOLZ patterns does not need the anomalous absorption in the many-beam approximation. The explanation is given by the Bloch-wave picture. The characteristic structure in the HOLZ patterns is caused by the high-indexed reflections from the first Laue zone. The density of the main Bloch wave oscillates very rapidly across the projection of the unit-cell on a plane parallel to the entrance surface owing to the high indices of the excited reflection. This results in a disappearance of the anomalous absorption effect and only a remaining mean absorption effect for this particular Bloch wave. Such a rapid oscillation of the Bloch-wave density was previously shown in an analysis of convergent-beam reflection electron diffraction experiments (Lehmpfuhl & Dowell, 1986). Simulations have been performed with absorption and modified Debye–Waller factor for lower and higher temperatures in order to obtain agreement with the experimental observations at 100 and 660 K with $D = 0.13$ and $1.0\,\text{Å}^2$ (Figs. 1*c*,*d*). They are shown in Figs. 4(*c*) and (*d*). The width of the separation of split HOLZ lines is reproduced with $D = 0.13\,\text{Å}^2$. The fine structure in Fig. 4(*d*) will be discussed below, together with the [100] observations.

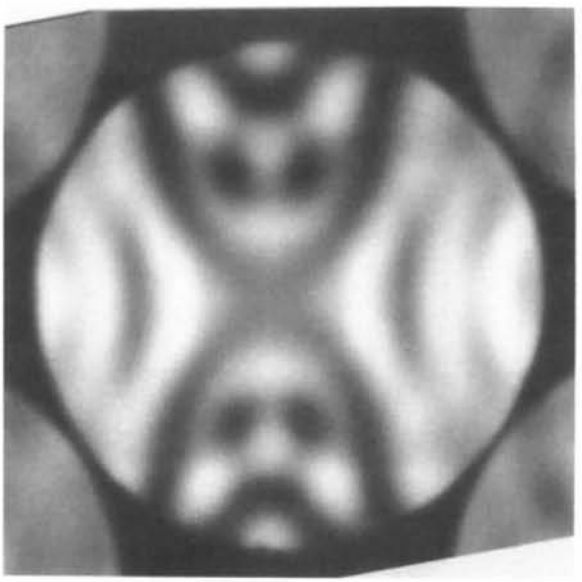

(*a*)

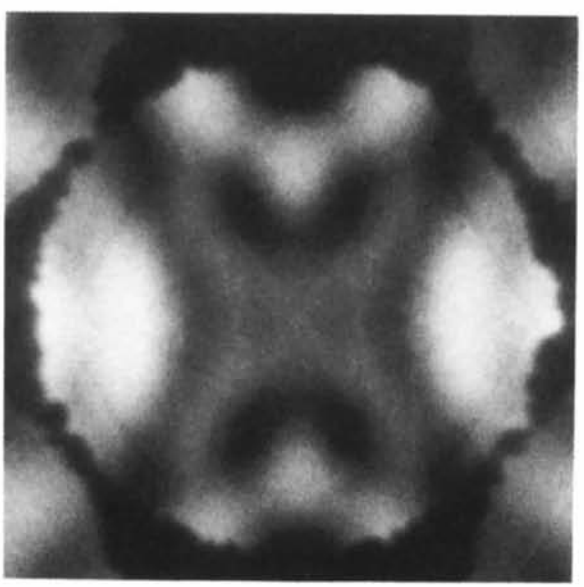

(*b*)

Fig. 3. (*a*) Energy-filtered zero beam of a convergent-beam pattern near the [110] zone axis at room temperature. No HOLZ lines are visible. (*b*) [110] HOLZ pattern at 50 K without energy filtering.

[100] *patterns*

The [100] zone-axis pattern in Fig. 2(*a*) shows fine lines with less contrast than the [111] HOLZ pattern. Again, the HOLZ lines were reproduced by calculations without absorption in Fig. 5(*a*). In the calculation with absorption and $D = 0.46\,\text{Å}^2$, however, complicated HOLZ-line profiles appear (Fig. 5*b*). The angular width of the calculated HOLZ-line fine structure is of the order of 10^{-5} rad, shown in high resolution in Fig. 5(*c*). The HOLZ lines show a maximum accompanied by two minima. The unexpected intensity anomalies were thought to be covered by inelastically scattered electrons in the experiment. However, in energy-filtered diffraction patterns such intensity anomalies could not be detected.

Calculations without absorption (Fig. 5*a*) did not show the intensity anomalies. They are, therefore, caused by the anomalous absorption. Previous investigations of diffraction experiments or the interpretation of electron microscopic observations have clearly shown the effect of anomalous absorption corresponding to the fact that each Bloch wave is absorbed with its own characteristic absorption coefficient, stated already by von Laue (1953). For X-ray diffraction, the anomalous absorption is known as the Borrmann effect (Borrmann, 1941). In electron diffraction, the anomalous absorption was treated by Molière (1939) by introducing an imaginary part in the structure potential, the absorption potential. Fourier coefficients of this absorption potential have been determined by the analysis of electron diffraction experiments (Ichimiya & Lehmpfuhl, 1988). The existence of this potential was confirmed by many observations, such as in the analysis of the fine structure of diffraction spots from a crystal wedge (Ishida, Johnson & Lehmpfuhl, 1975), which correspond to the *Pendellösung* fringes in electron microscopic images from crystal wedges (*e.g.* Uyeda, 1968).

This shows very clearly that the anomalous absorption is a well established phenomenon that cannot be simply neglected. Apparently, the mechanism of rapid Bloch-

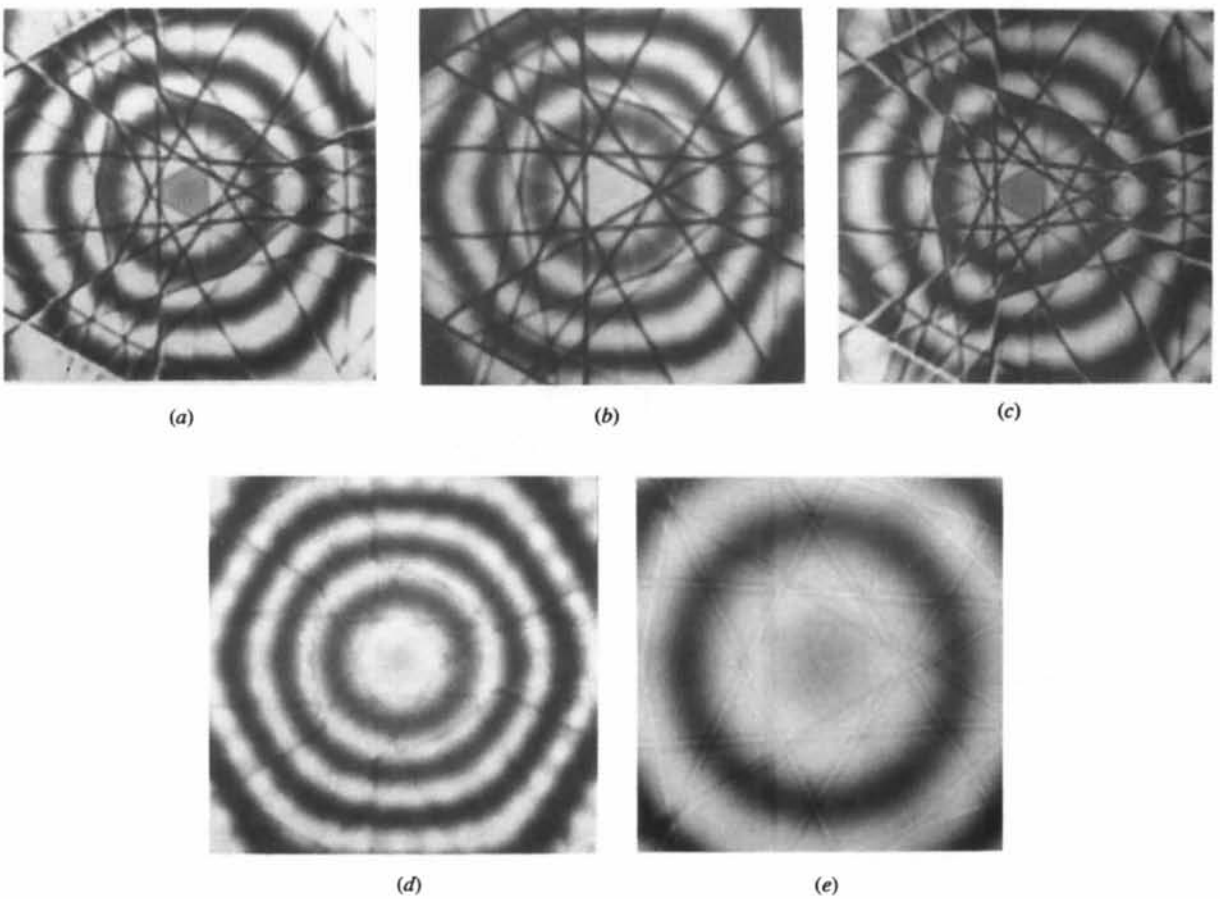

Fig. 4. (*a*) Zero-beam simulation of Si [111] HOLZ pattern with absorption in a 90-beam approximation with $D = 0.26\,\text{Å}^2$, wavelength = 0.003718 nm and thickness = 220 nm. (*b*) Zero-beam intensity simulation of the Si [111] HOLZ pattern without absorption. 90-beam approximation and $D = 0.46$ Å. (*c*) Zero-beam simulation of Si [111] HOLZ pattern with $D = 0.13\,\text{Å}^2$ corresponding to 110 K. (*d*) As (*c*) but with $D = 1.3\,\text{Å}^2$ corresponding to 660 K. (*e*) Zero-beam simulation of (*d*) with higher resolution.

wave oscillation mentioned above does not work in the calculation because of other reasons not yet known. Many reasons were considered to be responsible for the anomalies.

1. The assumption that the intensity artefacts were caused by the insufficient approximation of the treatment of absorption by perturbation calculation could be excluded by comparison with exact calculations with complex non-Hermitian matrices.

2. Modifications of the absorption model has also been tried. A steep decrease of the absorption potential with increasing scattering angle led to a better agreement between experiment and simulation. Such a steep decrease leads, however, to dominance of the remaining mean absorption and very little effect of anomalous absorption.

3. Another assumption why the artefacts were produced, namely the insufficient description of the

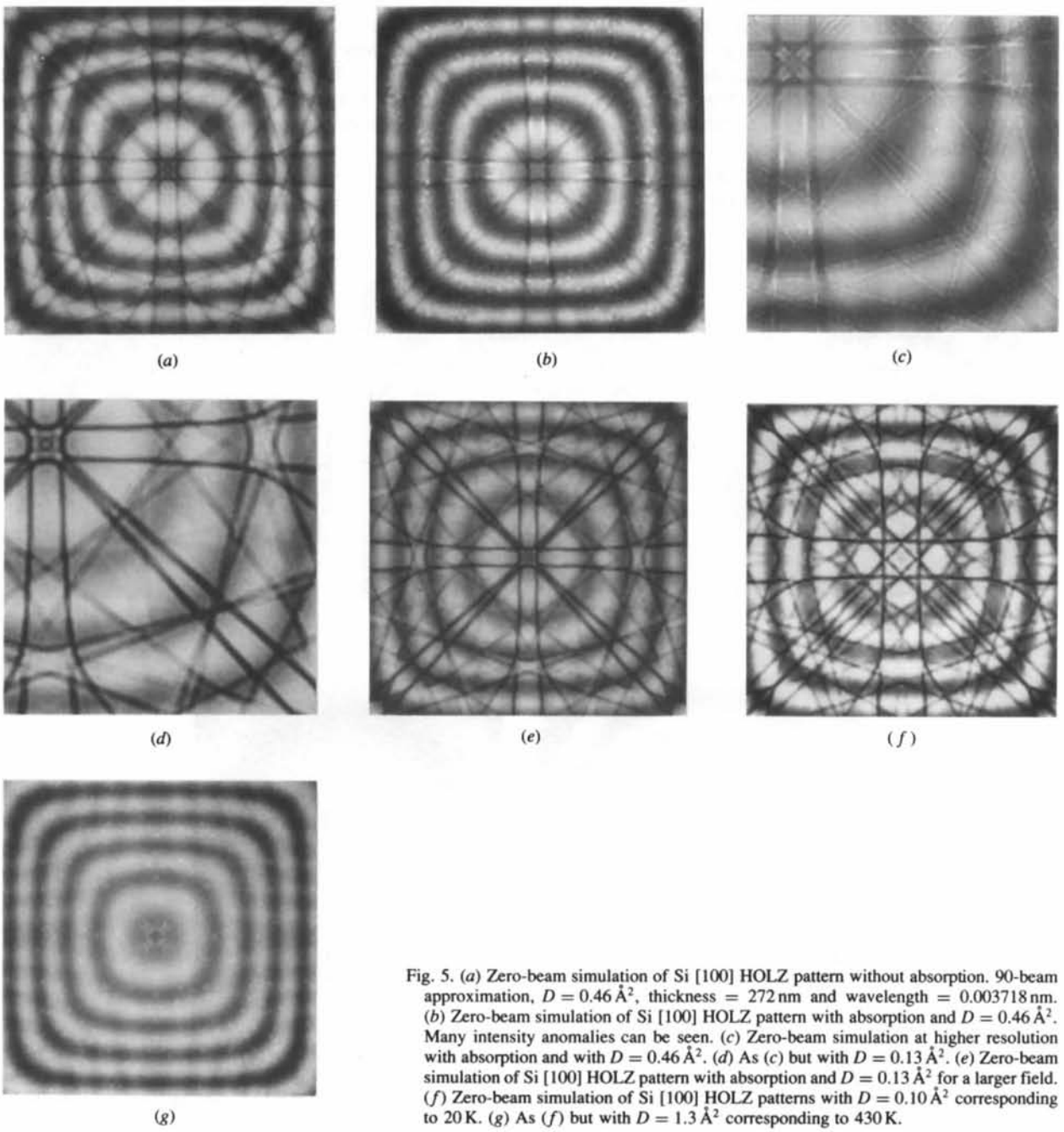

Fig. 5. (*a*) Zero-beam simulation of Si [100] HOLZ pattern without absorption. 90-beam approximation, $D = 0.46\,\text{Å}^2$, thickness = 272 nm and wavelength = 0.003718 nm. (*b*) Zero-beam simulation of Si [100] HOLZ pattern with absorption and $D = 0.46\,\text{Å}^2$. Many intensity anomalies can be seen. (*c*) Zero-beam simulation at higher resolution with absorption and with $D = 0.46\,\text{Å}^2$. (*d*) As (*c*) but with $D = 0.13\,\text{Å}^2$. (*e*) Zero-beam simulation of Si [100] HOLZ pattern with absorption and $D = 0.13\,\text{Å}^2$ for a larger field. (*f*) Zero-beam simulation of Si [100] HOLZ patterns with $D = 0.10\,\text{Å}^2$ corresponding to 20 K. (*g*) As (*f*) but with $D = 1.3\,\text{Å}^2$ corresponding to 430 K.

structure potential (Doyle & Turner, 1968) for the high-indexed Fourier coefficients for reflections of the first Laue zone, could also be excluded by calculations with the potential approximated by Cromer & Man (1968) leading to identical results.

4. An intensity minimum at the position of the HOLZ lines would be obtained by changing the phase of the absorption potential by 180°. However, this phase shift is not consistent with calculations for the [110] zone axis and leads to the wrong intensity asymmetry of the zero beam in convergent-beam electron diffraction patterns of systematic (111) excitation (Voss, Lehmpfuhl & Smith, 1980), which means that a phase shift is not realistic.

5. The Debye–Waller factor in the absorption potential also had no effect.

6. Refined values of the low-indexed structure potentials only have an influence on the intensity distributions due to reflections of the zeroth Laue zone as in the case of [110] shown below.

7. Changing the ratio of the number of reflections of the first Laue zone to the number of reflections of the zeroth Laue zone had no influence on the intensity anomalies.

We therefore had to look for other reasons for the intensity anomalies and ultimately found that, by reducing the value of D, the artefacts could almost be avoided, as shown with $D = 0.13$ Å^2 in Fig. 5(*d*). With $D = 0.46$ Å^2, the HOLZ lines in Fig. 5(*c*) showed a profile with a sharp detailed structure, as mentioned above, consisting of a maximum accompanied by two minima at the position where the HOLZ line would be expected. For a reduced value of D of 0.13 Å^2, the two accompanying minima dominate over the remaining decreased maximum as shown in Fig. 5(*d*). Calculations of the larger field with absorption and $D = 0.13$ Å^2 (Fig. 5*e*) show a very good agreement with the experiment. This result indicates a strong anisotropy of the Debye–Waller factor, which is supported by the following observation: the HOLZ-line profile in the simulated [111] zone-axis pattern at an elevated temperature of 660 K with $D = 1.3$ Å^2 (Fig. 4*e*) looks similar to the line profile of the [100] zone-axis pattern calculated with $D = 0.46$ Å^2 (Fig. 5*d*) (Voss, Lehmpfuhl & Smith, 1980; Aldred & Hart, 1973). Starting from this situation in [111], one has to decrease the value of D down to $D = 0.26$ Å^2 to obtain agreement with the experimental observation at room temperature; for [100], D had to be 0.13 Å^2 at this temperature.

The simulations at the elevated temperature of 430 K with $D = 1.3$ Å^2 (Fig. 5*g*) and at 660 K with $D = 1.3$ Å^2 for [111] (Fig. 4*d*) are in reasonable agreement with the experimental observation in Figs 2(*d*) and 1(*d*). Remaining artefacts in the calculation have an angular width of the order of less than 2×10^{-5} rad, which would correspond to a diffraction angle from a lattice with a separation of 190 nm or from a coherent scattering area of this dimension. The question arises if such fine details can be resolved in the diffraction pattern experimentally. We consider two reasons for a limitation of the resolution: (i) the size of the crystal area contributing coherently to the diffraction pattern; (ii) the orientation of the entrance surface of the crystal which leads to an effect of refraction. If the (100) surface is formed by (110) or (111) facets, the remaining artefacts are smeared over a larger area and so they disappear. This would explain the smooth intensity with weak HOLZ lines in the experimental patterns in Figs. 2(*d*) and 1(*d*). Calculations without absorption but with the same value of D show such an intensity distribution.

Simulation of HOLZ lines for 20 K needed a very small value of D to reproduce the many lines observed in the experiment. Fig. 5(*f*) shows a simulation with $D = 0.1$ Å^2. This variation of contrast with temperature again confirms the anisotropy of the Debye–Waller factor.

[110] *patterns*

The [110] zone-axis pattern does not show any HOLZ lines at room temperature but a characteristic intensity distribution that depends strongly on thickness. The reflections of the first Laue zone have very high indices so that they are too weak to modify the intensity of the zero beam. Even after energy filtering, they cannot be seen. In order to reproduce this pattern by simulation, the correct absorption (Voss, Lehmpfuhl & Smith, 1980) has to be used since the intensity distribution is mainly influenced by reflections of the zeroth Laue zone. Furthermore, the forbidden reflections, *e.g.* 200, have to be taken into account. They are excited by *Umweganregung*. The value of the low-order structure potential such as 111 is also important for this calculation. The experimentally refined value for the 111 structure potential (Voss *et al.*, 1980) was therefore used in the simulation instead of the Doyle–Turner value (Doyle & Turner, 1968). The optimized simulation with a 120-beam calculation and a D value of the Debye–Waller factor $D = 0.55$ Å^2 is shown in Fig. 6(*a*). The agreement with the experiment in Fig. 3(*a*) is fairly good. It should be mentioned here that, in a 90-beam simulation and with $D = 0.46$ Å^2, no HOLZ lines appeared but in a better approximation with 180 beams they appeared again. This may be due to the number of beams of the first Laue zone included by the election procedure. Since at room temperature no HOLZ lines could be detected in the energy-filtered pattern, the value of D is larger than 0.46 Å^2, as confirmed by the simulation with $D = 0.55$ Å^2 in Fig. 6(*a*). This result again shows an anisotropy of the Debye–Waller factor for silicon.

In order to reproduce [110] HOLZ lines at low temperature with reasonable contrast, the Debye–Waller factor had to be reduced to $D = 0.1$ Å^2. The result is shown in Fig. 6(*b*). The agreement with the experiment in Fig. 3(*b*) is fairly good. The arrangement of the [110] HOLZ lines is most sensitive to the wavelength of the

electrons compared with the other zone axes. The contrast of the HOLZ lines in the experiment is reduced by inelastically scattered electrons.

During this analysis, a very surprising result was found for the [110] zone axis, which may help to improve the understanding of the scattering process. For each direction of incidence, the reflections used in the calculation are selected by a selection procedure as mentioned above. This leads to distinct numbers of reflections from the zeroth and the first Laue zones. The zone-axis pattern of the optimized 120-beam calculation in Fig. 6(*a*) does not show any HOLZ lines. However, when reducing the number of beams to 30, HOLZ lines appear very clear as can be seen in Fig. 6(*c*). In order to get rid of them in such an approximation, one would have to increase the Debye–Waller factor. The physical background in this observation is, however, that in a 30-beam approximation the influence of the reflections of the first Laue zone on the intensity of the zero beam is overestimated, leaving a non-realistic increase of HOLZ-line contrast. With 90 or more beams, however, the contrast becomes more realistic. When using a very large number of beams in the calculation, it should be possible to determine the correct Debye–Waller factor. Otherwise, the Debye–Waller factor would act as a fitting parameter to compensate for the artefacts produced by an insufficient approximation.

Summary of comparison

The investigations have clearly shown that a strong anisotropy of the Debye–Waller factor for silicon at different temperatures has to be assumed to reproduce the HOLZ lines in different zone axes. The results are shown in Table 1 and Fig. 7. The non-linear temperature dependence and the direction-dependent temperature

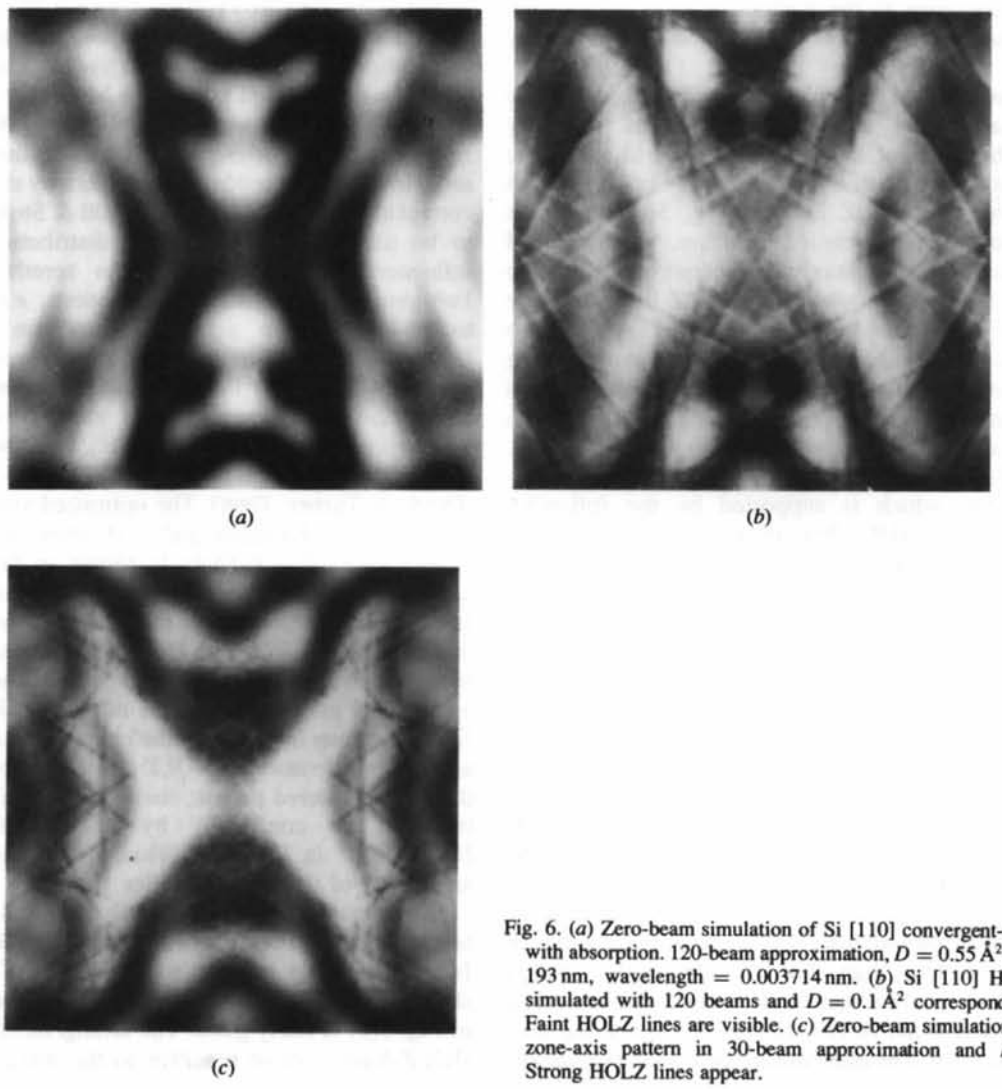

(*a*) (*b*) (*c*)

Fig. 6. (*a*) Zero-beam simulation of Si [110] convergent-beam pattern with absorption. 120-beam approximation, $D = 0.55$ Å^2, thickness = 193 nm, wavelength = 0.003714 nm. (*b*) Si [110] HOLZ pattern simulated with 120 beams and $D = 0.1$ Å^2 corresponding to 50 K. Faint HOLZ lines are visible. (*c*) Zero-beam simulation of Si [110] zone-axis pattern in 30-beam approximation and $D = 0.55$ Å^2. Strong HOLZ lines appear.

Table 1. *D values in* Å^2 *for different zone axes and different temperatures*

	[100]	[111]	[110]
20 K	0.10	–	–
50 K	–	–	0.1
100 K	–	0.13	–
Room temp.	0.13	0.26	0.55
430 K	1.3	–	–
600 K	–	1.3	–

factor shown in Fig. 7 are the most exciting results of this work. They contradict results of the well established determination of the Debye–Waller factor using diffraction techniques with X-rays (*e.g.* Batterman, 1962), electrons (*e.g.* Swaminathan *et al.*, 1994) or neutrons (*e.g.* Zhang *et al.*, 1990). The analysis is based upon kinematical or dynamical diffraction processes of the zeroth Laue zone. In our analysis, the more complete sets of reflections of the zeroth and the first Laue zone had been considered, and in this case the Debye–Waller factor had to be modified to simulate the HOLZ lines leading to the strong anisotropy.

It is well known that the crystal symmetry restricts the symmetry of the temperature factor. The Debye–Waller factor for a crystal with cubic symmetry should be isotropic. This fact is only valid for harmonic crystals. Anharmonic contribution to the Debye–Waller factor has been theoretically investigated by Maradudin & Flinn (1963), Willis (1969) and Willis & Pryor (1975), and the possibility of an anisotropic temperature factor for the cubic crystal has been found. In addition to this, the silicon crystal has a diamond structure. All atoms are situated at the sites of tetrahedral symmetry (a point group $\bar{4}3m$). The potential of an atom in this crystal has, as well as the isotropic term, a term with tetrahedral symmetry. This can be easily understood by the picture of the equipotential surface for one atom where the spherical form (the harmonic term) is modified with four tetrahedral lobes in the [111] directions. This means that the atoms in the crystal are more rigid in [111] directions than in other directions. Therefore, the atomic displacement due to thermal vibration in these directions may be smaller than in other directions. The unexpected large anisotropy of the temperature factor cannot be explained with the anharmonic crystal potential because of its small fraction from the harmonic effect. The inversion of the factors for the [111] and [100] axes between room temperature and higher temperatures cannot be explained. The more isotropic behaviour at low temperatures may be due to less anharmonicity.

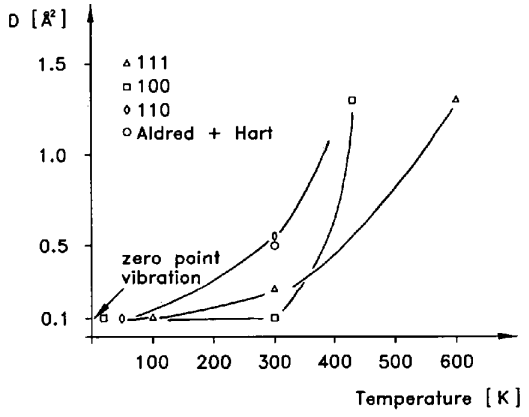

Fig. 7. Temperature dependence of the *D* values (Table 1) for the different zone axes.

Concluding remarks

The characteristic structure of zone-axis patterns can be generated by the first Laue zone or only by the zeroth Laue zone. In the first case, we call them HOLZ patterns. This depends on the scattering angle for the reflections of the first Laue zone corresponding to the sum of the squares of their indices. At the [110] azimuth, the first Laue zone is furthest away. The reflections have very high indices with a sum of their squares proportional to s^2 in (3),

$$\mathrm{SQ} = (h^2 + k^2 + l^2),$$

of the order of 400 (depending on the wavelength). For the other zone axes, such as [100], this sum is of the order of 300 and for [111] only 170. Owing to the indices of the reflections of the first Laue zone, the influence of the Debye–Waller factor is expected to be largest for the [110] zone axis.

The unexpected result, that without absorption the agreement between experiment and calculation is excellent for the two zone axes [111] and [100], is because here the characteristic structure of the pattern comes from the reflections of the first Laue zone. With these high-order reflections, characteristic Bloch waves are excited and are damped by a mean absorption.

The characteristic features of the intensity distribution in the [110] HOLZ pattern, however, are generated at room temperature only by reflections of the zeroth Laue zone. Consequently, a simulation needs dynamical calculation with the correct absorption potential.

Summary

Intensity anomalies in calculated [100] HOLZ patterns were investigated. They could not be detected experimentally. Many possibilities for their production were considered starting with insufficient approximation for solving the fundamental equations of the dynamical theory with the complex potential due to absorption. Other possibilites, such as contribution of inelastic scattering, insufficient number of beams, selection procedure of relevant reflections, model of absorption, phase of absorption and influence of the Debye–Waller factor in the absorption potential, could also be excluded. A consequent interpretation of these facts, together with the observations in this paper and other papers, leads to an anisotropy of the Debye–Waller factor for silicon and,

furthermore, to a temperature dependence of the Debye temperature. For this analysis, the use of an imaging energy filter was essential.

This result is important for a general structure determination by diffraction techniques when interactions of reflections from higher-order Laue zones have to be considered. Another conclusion would be that the intentensity anomalies should be observable with a perfect crystal with atomically flat surfaces in an energy-filtered pattern.

We thank Dr K. Kambe for many discussions and for his permission to use the perturbation program. We also thank Professor A. Ichimiya for his suggestions. Mrs H. Sack-Kongehl and Mr K. Weiss are thanked for plotting the simulations, Mr J. Kühn for his help in the application of the computer equipment, and Dr A. Preusser for helping us with the complex matrix calculation.

References

ALDRED, P. J. & HART, M. (1973). *Proc. R. Soc. London Ser. A*, **332**, 223–254.
BATTERMAN, B. W. (1962). *Phys. Rev.* **127**, 686–690.
BORRMANN, G. (1941). *Phys. Z.* **42**, 157.
CROMER, D. T. & MANN, J. B. (1968). *Acta Cryst.* A**24**, 321–324.
DOYLE, P. & TURNER, A. (1968). *Acta Cryst.* A**24**, 390–397.
GOODMAN, P. (1974). *Acta Cryst.* A**28**, 92–93.
GOODMAN, P. & LEHMPFUHL, G. (1965). *Z. Naturforsch. Teil A*, **20**, 110–114.
HEIDE, H. G. (1982). *Ultramicroscopy*, **10**, 125–154.
HOLMESTAD, R., KRIVANEK, O. L., HØIER, R., MARTHINSEN, K. & SPENCE, J. C. H. (1993). *Ultramicroscopy*, **52**, 454–458.
HUMPHREYS, C. J. & HIRSCH, P. B. (1968). *Philos. Mag.* **18**, 115–122.
ICHIMIYA, A. & LEHMPFUHL, G. (1978). *Z. Naturforsch. Teil. A*, **33**, 269–281.
ICHIMIYA, A. & LEHMPFUHL, G. (1988). *Acta Cryst.* A**44**, 806–809.
ISHIDA, K., JOHNSON, A. R. & LEHMPFUHL, G. (1975). *Z. Naturforsch. Teil A*, **30**, 1715–1729.
KAMBE, K. & MOLIÈRE, K. (1970). *Advances in Structure Research by Diffraction Methods*, Vol. 3, edited by R. BRILL & R. MASON, p. 53. Oxford: Pergamon Press.
KRAHL, D. (1990). *Mater. -wiss. Werkst.* **21**, 84–90.
LAUE, M. VON (1953). *Acta Cryst.* **6**, 217–218.
LEHMPFUHL, G. & DOWELL, W. C. T. (1986). *Acta Cryst.* A**42**, 569–577.
MARADUDIN, A. A. & FLINN, P. A. (1963). *Phys. Rev.* **129**, 2529–2547.
MAYER, J., SPENCE, J. C. H. & MÖBUS, G. (1991). *Proceedings of Electron Microscopy Society of America*, edited by G. BAILEY, pp. 786–787. San Francisco Press.
MOLIÈRE, K. (1939). *Ann. Phys. (Leipzig)*, **34**, 461–472.
RACKHAM, G. M., STEEDS, J. W. & JONES, P. M. (1975). *Acta Cryst.* A**31**, S252–S253.
REIMER, L. (1989). *Transmission Electron Microscopy, Springer Series in Optical Science*, Vol. 36, p. 316. Berlin: Springer.
STEEDS, J. W. & JONES, P. M. (1975). *Acta Cryst.* A**31**, S252.
SWAMINATHAN, S., ALTYNOV, S., JONES, I. P., ZALUZEC, N. J., MAHER, D. M. & FRASER, H. L. (1994). Proc. 13th International Congress on Electron Microscopy, Paris, Vol. 1, pp. 861–862.
TANAKA, M., TERAUCHI, M. & KANEYAMA, T. (1985). *Convergent Beam Electron Diffraction*, Vols. I and II. JEOL Ltd, 1418 Nakagami, Akashima, 196 Japan.
UYEDA, R. (1968). *Acta Cryst.* A**24**, 175–181.
VOSS, R., LEHMPFUHL, G. & SMITH, P. (1980). *Z. Naturforsch. Teil A*, **35**, 973–984.
WILLIS, B. T. M. (1969). *Acta Cryst.* A**25**, 277–300.
WILLIS, B. T. M. & PRYOR, A. W. (1975). *Thermal Vibration in Crystallography*. Cambridge Univ. Press.
ZHANG, B., YANG, J., JIN, L., YE, C., BASHIR, J., BUTT, N. M., SIDDIQUE, M., ARSHED, M. & KHAN, Q. H. (1990). *Acta Cryst.* A**46**, 435–437.
ZHOU, F. (1991). Private communication.
ZHOU, F. & MÖLLENSTEDT, G. (1992). *Ultramicroscopy*, **41**, 359–366.

Acta Cryst. (1995). A**51**, 514–519

Cation Ordering Waves in Trirutiles. When X-ray Crystallography Fails?

BY STAFFAN HANSEN* AND ANGEL LANDA-CÁNOVAS

National Center for HREM, Inorganic Chemistry 2, Chemical Center, University of Lund, PO Box 124, S-221 00 Lund, Sweden

KENNY STÅHL

Inorganic Chemistry 2, Chemical Center, University of Lund, PO Box 124, S-221 00 Lund, Sweden

AND JERKER NILSSON

Chemical Technology, Chemical Center, University of Lund, PO Box 124, S-221 00 Lund, Sweden

(*Received 27 December 1994; accepted 13 March 1995*)

Abstract

Trirutiles are AB_2O_6 crystal structures with a tripled *c*-axis repeat compared to the rutile type, owing to *ABBABBA* metal ordering. Partially disordered trirutiles, space group $P4_2/mnm$, are here described by addition of a sinusoidal scattering density wave along **c** to the basic rutile structure. As a result of this approach, an infinite number of crystal structures can be envisaged, which

* To whom all correspondence should be addressed.